Eur. Phys. J. A (2021) 57:157
https://doi.org/10.1140/epja/s10050-021-00465-0

THE EUROPEAN PHYSICAL JOURNAL A

Regular Article - Theoretical Physics

α clustering and neutron-skin thickness of carbon isotopes

Q. Zhao[1], Y. Suzuki[2], J. He[2], B. Zhou[2,3], M. Kimura[1,2,4,a]

[1] Nuclear Reaction Data Centre (JCPRG), Hokkaido University, Sapporo 060-0810, Japan
[2] Department of Physics, Hokkaido University, Sapporo 060-0810, Japan
[3] Institute of Modern Physics, Fudan University, Shanghai 200433, China
[4] Research Center for Nuclear Physics (RCNP), Osaka University, Ibaraki 567-0047, Japan

Received: 23 February 2021 / Accepted: 12 April 2021

Communicated by David Blaschke

Abstract The interplay between the formation of neutron skin and α cluster at the dilute surface of neutron-rich nuclei is one of the interesting subjects in the study of neutron-rich nuclei and nuclear clustering. A theoretical model has predicted that the growth of neutron skin will prevent the α clustering at nuclear surface. Quite recently, this theoretical perspective, the suppression of α clustering by the neutron-skin formation, was firstly confirmed experimentally in Sn isotopes as the reduction of the $(p, p\alpha)$ reaction cross section. Motivated by the novel discovery, in this work, we have investigated the relationship between the neutron-skin thickness and α clustering in C isotopes. Based on the analysis by the antisymmetrized molecular dynamics, we show that the α spectroscopic factor at nuclear exterior decreases in neutron-rich C isotopes, and the clustering suppression looks correlated with the growth of the neutron-skin thickness.

1 Introduction

It has been theoretically expected that the formation of α clusters in dilute nuclear matter is dependent not only on nuclear density, but also on the symmetry energy [1,2]. Accordingly, in finite nuclei, we also expect that the neutron-skin affects α clustering at nuclear exterior. A theoretical model study [3] has predicted the suppression of surface α clustering in neutron-rich nuclei due to the growth of neutron skin.

Recently, the α knockout $(p, p\alpha)$ reaction has been established as a quantitative probe for the α clustering at nuclear surface [4–7], and using this reaction, the α cluster formation at the surface of Sn isotope chain has been measured for the first time [8]. It has been shown that the knockout cross section monotonically decreases in neutron-rich Sn isotopes indicating the negative correlation between the neutron skin formation and α clustering. Hence, the growth of neutron skin looks preventing the α clustering at the surface of heavy nuclei.

Motivated by this fascinating discovery, we investigate the relationship between the neutron-skin thickness and α clustering in C isotopes. The advantages of studying light carbon isotopes is in reducing the theoretical uncertainty about nuclear clustering. The consistent description of α clusters and neutron skin within the same theoretical framework is, in general, still challenging [9,10]. However, there are ample theoretical and experimental studies for C isotopes and its core nuclei (Be isotopes) [11–13], and their low-lying spectra have been established well. Furthermore, the decades of the studies have revealed the α clustering of ^{12}C in detail [14–17]. Thanks to these prior knowledge, we are able to make a quantitative anatomy of the relationship between the neutron skin and α clustering for C isotopes.

This paper is organized as follows. In the next section, the theoretical framework of the antisymmetrized molecular dynamics (AMD) [12,13,18] used to calculate the wave functions of Be and C isotopes, and the method to evaluate the α spectroscopic factors are briefly explained. In the Sect. 3, we present the numerical results and discuss the relationship between the neutron-skin thickness and α clustering. It has been found that the α clustering of C isotopes likely show the negative correlation with the neutron-skin thickness similarly to Sn isotopes. The final section summarizes this work.

2 Theoretical framework

2.1 Hamiltonian and model wave function

The microscopic A-body Hamiltonian is used in this study. It reads,

[a] e-mail: masaaki@nucl.sci.hokdai.ac.jp (corresponding author)

Published online: 04 May 2021

$$H = \sum_{i}^{A} t_i - t_{\rm cm} + \frac{1}{2}\sum_{ij}^{A} v_{\rm NN}(ij) + \frac{1}{2}\sum_{ij\in{\rm proton}}^{Z} v_{\rm C}(ij), \quad (1)$$

where the Gogny D1S parameter set [19] is employed as nuclear density functional $v_{\rm NN}(ij)$, and the Coulomb interaction $v_{\rm C}(ij)$ is approximated by a sum of seven Gaussians as explained in the appendix. The center-of-mass kinetic energy $t_{\rm cm}$ is subtracted from the total energy without any approximation.

The model wave function is a parity-projected Slater determinant,

$$\Phi^{\pi} = P^{\pi}\mathcal{A}\{\varphi_1\varphi_2\dots\varphi_A\}, \quad (2)$$

where P^{π} denotes parity projector, and φ_i is the nucleon wave packet expressed by deformed Gaussian [20],

$$\varphi_i(\boldsymbol{r}) = \exp\left\{-\sum_{\sigma=x,y,z}\nu_\sigma\,(r_\sigma - Z_{i\sigma})^2\right\}\chi_i\tau_i, \quad (3)$$

$$\chi_i = a_i\chi_\uparrow + b_i\chi_\downarrow, \quad \tau_i = \{\text{proton or neutron}\}. \quad (4)$$

The parameters of the model wave function are the Gaussian widths (ν_x, ν_y, ν_z), centroids $\boldsymbol{Z}_i$, and the spin direction a_i and b_i. They are determined by the frictional cooling method which minimizes the sum of the Hamiltonian and constraint potential,

$$E(\beta) = \frac{\langle\Phi^{\pi}|H|\Phi^{\pi}\rangle}{\langle\Phi^{\pi}|\Phi^{\pi}\rangle} + v_\beta(\langle\beta\rangle - \beta)^2, \quad (5)$$

where the constraint potential strength v_β is chosen sufficiently large value so that the deformation of the model wave function $\langle\beta\rangle$ [21] is equal to the input value β by the minimization of $E(\beta)$. And we obtain the optimized wave function $\Phi^{\pi}(\beta)$ which has the minimum energy for each given value of β.

After the energy variation, the optimized wave functions are projected to the eigenstate of the angular momentum,

$$\Phi^{J\pi}_{MK}(\beta) = \frac{2J+1}{8\pi^2}\int {\rm d}\Omega\, D^{J*}_{MK}(\Omega)R(\Omega)\Phi^{\pi}(\beta), \quad (6)$$

where $D^{J}_{MK}(\Omega)$ and $R(\Omega)$ denote the Wigner's D-function and the rotation operator. Then, the projected wave functions which have different value of the deformation parameter β are superposed as,

$$\Psi^{J\pi}_{\alpha} = \sum_{iK} g_{iK\alpha}\Phi^{J\pi}_{MK}(\beta_i). \quad (7)$$

Namely, Eq. (7) is the wave function of the generator coordinate method (GCM) [22] which employs the deformation parameter β as the generator coordinate. The coefficients $g_{iK\alpha}$ and eigenenergy E_α are obtained by solving the Hill-Wheeler equation [22],

$$\sum_{jK'}(H_{iKjK'} - E_\alpha N_{iKjK'})g_{jK'\alpha} = 0 \quad (8)$$

$$H_{iKjK'} = \langle\Phi^{J\pi}_{MK}(\beta_i)|H|\Phi^{J\pi}_{MK'}(\beta_j)\rangle, \quad (9)$$

$$N_{iKjK'} = \langle\Phi^{J\pi}_{MK}(\beta_i)|\Phi^{J\pi}_{MK'}(\beta_j)\rangle. \quad (10)$$

From the GCM wave functions, we calculate the properties of C isotopes such as the excitation spectra, proton and neutron distribution radii and electric transition probabilities.

2.2 α reduced width amplitude

To evaluate the degree of α clustering in C isotopes, we calculate α reduced width amplitude (RWA) from the GCM wave functions. It is the probability amplitude to find α cluster at distance a from the daughter nucleus, and is defined as

$$a y_\ell(a) = \sqrt{\tbinom{A}{4}}\langle\delta(r-a)\Phi_\alpha[\Phi_{{\rm Be}(\ell^+)}Y_\ell(\hat{r})]_0|\Phi_{\rm C}\rangle, \quad (11)$$

where Φ_α, $\Phi_{{\rm Be}(\ell^+)}$ and $\Phi_{\rm C}$ are the fully-antisymmetrized wave functions of α cluster, the ground and excited states of Be isotopes with spin-parity ℓ^+ and the ground state of C isotopes, respectively. The wave functions of Be and C isotopes are calculated by the AMD+GCM framework explained in the previous section, while that of α cluster is a product of Gaussians whose size parameter is chosen to reproduce the observed value of the ^{4}He radius. Note that the angular momentum ℓ of the orbital motion between α and Be isotope, and the spin of Be isotopes which is also ℓ are coupled to the total angular momentum zero. In other words, we calculate α RWA in the $\ell^+\times\ell = 0^+\times 0, 2^+\times 2$ and $4^+\times 4$ channels ($\ell \le 4$), where the first number represents the spin of Be isotope and the second number represents the orbital angular momentum between α and Be isotope. In the practical numerical calculation, Eq. (11) has been evaluated by using the Laplace expansion method [23]. We also comment about the size of α cluster. In general, the size of α cluster at the nuclear surface might be different from that in free space. However, we have confirmed that the size change of α cluster is negligibly small at the surface of several light nuclei and does not affect the magnitude of the α spectroscopic factors [23]. Therefore, in the present study, we have assumed that the α cluster size at the nuclear surface is the same with that in free space, although the systematic study of the size change effect in various isotopes is an interesting issue.

The degree of the α clustering may be evaluated by the so-called α spectroscopic factor which is the squared integral of the α RWA,

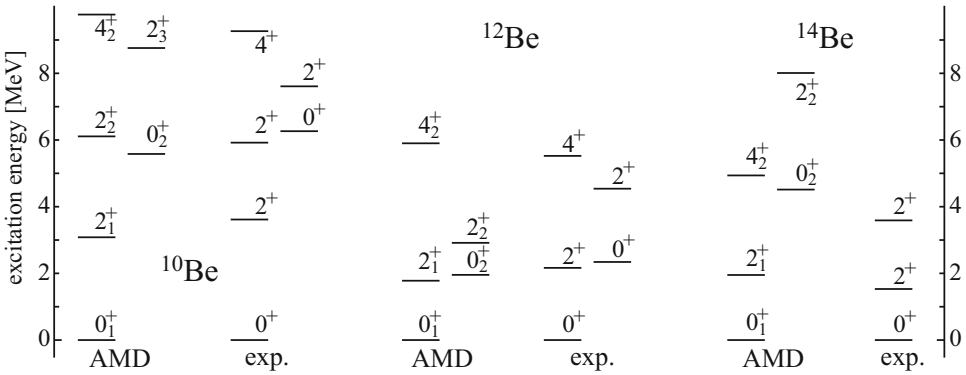

Fig. 1 The calculated low-lying spectra of Be isotopes compared with the experimental data [28–30]. Only the positive-parity states are shown

$$S_\alpha(\ell^+ \times \ell) = \int_0^\infty r^2 dr\ y_\ell^2(r). \tag{12}$$

It is noted that S_α is not normalized unity because of the anti-symmetrized effects between the α cluster and Be isotopes. As already discussed in the preceding studies [6,7], the α knockout reaction is sensitive only to the α particle formed at the nuclear surface. Therefore, we expect that the integral of α RWA in nuclear exterior is a good measure for the knockout cross section. So, we introduce the α spectroscopic factor integrated only in the exterior region,

$$S_\alpha^>(\ell^+ \times \ell) = \int_{\sqrt{\langle r_m^2\rangle}}^\infty r^2 dr\ y_\ell^2(r), \tag{13}$$

where $\sqrt{\langle r_m^2\rangle}$ denotes the root-mean-square radii of matter distribution of C isotopes.

3 Results and discussions

3.1 Structure of Be and C isotopes

The structure of neutron-rich Be and C isotopes has already been studied in detail within the AMD model and is summarized in the review papers [11,13]. Therefore, we do not go into detail here, but only explain the important points necessary for the discussion of α clustering.

Firstly, we note that this is the first systematic calculation of both Be and C isotopes using the Gogny D1S density functional, and it plausibly and consistently describes the low-lying spectra as shown in Figs. 1 and 2. This encouraging result ensures the reliability of the analysis of the α cluster formation presented in the next section.

As is well known, all calculated Be isotopes have dumbbell-shaped structure due to the pronounced 2α clustering [33,34]. This brings about the strong deformation and $B(E2\uparrow)$ of the ground states (Table 1). If we investigate the property of individual isotope a little closer, we notice that ^{12}Be and ^{14}Be are more deformed than ^{10}Be. This is due to the difference of the valence neutron orbits in these

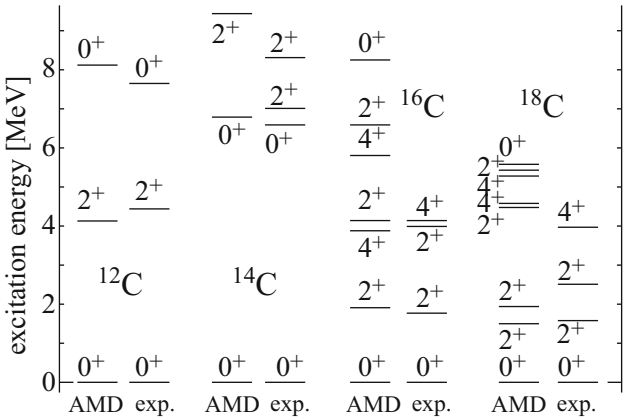

Fig. 2 Same with Fig. 1 but for C isotopes. Experimental data are taken from Refs. [29–32]

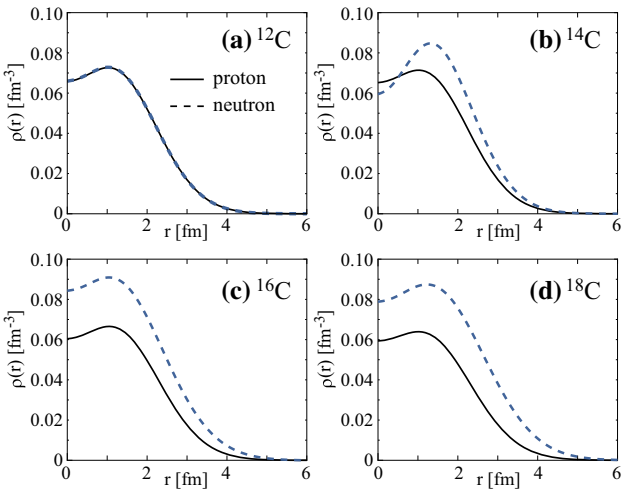

Fig. 3 The calculated point proton and neutron density distributions of the ground states of C isotopes. The densities are normalized to the particle numbers

isotopes. Namely, two valence neutrons of ^{12}Be and ^{14}Be occupy the sd-shell [11]. On the other hand, all valence neutrons of ^{10}Be occupy the $0p$ orbits which tend to reduce the inter-cluster distance. Note that our calculation reproduces the well-known breaking of $N = 8$ magic number [35] in

Table 1 The deformation parameter β; the $E2$ transition probability; the proton, neutron and matter distribution radii; and the α spectroscopic factors for $\ell = 0$ channel of the calculated ground states of Be and C isotopes. The $B(E2)$ values are given in the unit of $e^2\text{fm}^4$, while the proton, neutron, matter radii and neutron-skin thickness Δr are given in the unit of fm

	β	$B(E2\uparrow)$	$B(E2\uparrow)_{\text{obs}}$	$\sqrt{\langle r_p^2\rangle}$	$\sqrt{\langle r_n^2\rangle}$	$\sqrt{\langle r_m^2\rangle}$	Δr	$S_\alpha(0_1^+ \times 0)$	$S_\alpha^>(0_1^+ \times 0)$
^{10}Be	0.56	56.0	46.7	2.43	2.50	2.47	0.07		
^{12}Be	0.60	60.3	40.0	2.63	2.91	2.82	0.28		
^{14}Be	0.59	64.0		2.64	3.03	2.92	0.40		
^{12}C	0.50	56.0	39.7	2.52	2.52	2.52	0.00	0.30	0.24
^{14}C	0.34	14.2	18.7	2.54	2.59	2.57	0.05	0.10	0.08
^{16}C	0.39	18.0	3.3 [24], 13.5 [25] 23.0 [26]	2.60	2.83	2.74	0.23	0.05	0.04
^{18}C	0.45	23.0	21.5 [25], 18.2 [27]	2.65	2.98	2.87	0.33	0.04	0.04

^{12}Be as two neutrons are promoted into sd-shell from p-shell across $N = 8$ shell gap. We also note that difference in the valence neutron configuration is clearly reflected to the neutron distribution radii $\sqrt{\langle r_n^2\rangle}$. As a result, the neutron-skin thickness $\Delta r = \sqrt{\langle r_n^2\rangle} - \sqrt{\langle r_p^2\rangle}$ continuously increases toward the neutron-drip-line nucleus ^{14}Be.

We also comment on the non-yrast states of ^{10}Be and ^{12}Be. ^{10}Be has the 2_2^+ state approximately at 6 MeV which is reproduced by our calculation. This state has the same single-particle configuration with the ground state but originates in the triaxial deformation of its intrinsic structure [36]. On the other hand, the 0_2^+ and 2_3^+ states of ^{10}Be have the internal structure different from the ground state. Namely, these are the neutron $2\hbar\omega$ excited states in which two neutrons are promoted into sd-shell across $N = 8$ shell gap. The opposite occurs in ^{12}Be whose ground state is dominated by the $2\hbar\omega$ configuration as already mentioned, but its non-yrast states (the 0_2^+ and 2_2^+ states) are dominated by the $0\hbar\omega$ state with the $N = 8$ closed shell configuration. Thus, the present calculation reasonably reproduces the known characteristics of the low-lying states of Be isotopes.

Next, we discuss the spectra of C isotopes shown in Fig. 2. Because of the $Z = N = 6$ sub-shell closure and $N = 8$ shell closure, ^{12}C and ^{14}C are rather stiff and have large excitation energies of the 0^+ and 2^+ states. On the contrary, ^{16}C and ^{18}C are rather soft and have many low-lying states, as they are weakly bound and have extra neutrons in an open shell (sd-shell). It is notable that the present calculation reasonably described the excitation spectra of both stiff and soft nuclei. Another interesting point to be noted is that all C isotopes except for ^{12}C have small $B(E2\uparrow)$ values despite their non-small quadrupole deformation [13,37,38] as listed in Table 1. This result is consistent with the trend of the observed $E2$ transitions [24–27] and indicates that the 2_1^+ states of C isotopes are dominated by neutron excitation not by proton excitation [39].

The neutron single-particle configuration also affects the neutron-skin thickness (Table 1 and Fig. 3). The neutron skin of ^{14}C is negligibly thin as two excess neutrons occupy the same major shell (p-shell) with protons. In ^{16}C and ^{18}C, the excess neutrons start to occupy sd-shell, which pushes the neutron density distributions outwards as seen in Fig. 3. Because of the deformation, the valence neutron wave function is not a pure $d_{5/2}$ but an admixture of the d- and s-wave components. This can be confirmed as the increase of the central density of ^{16}C and ^{18}C compared to ^{14}C. More quantitatively, by the multipole decomposition of the single-particle orbits [40], we estimate that the neutron $(1s)^2$ configuration amounts to 23% of the ^{16}C ground state, whereas the neutron $(0d_{5/2})^2$ and $(0d_{3/2})^2$ configurations are 43% and 21%, respectively. These are not far from an estimate by a large scale shell model calculation [41]; 22.4% from the $(1s)^2$ configuration and 22.6% from the $(0d_{5/2})^2$ configuration. For ^{18}C, we also obtained similar magnitude of the occupation probabilities; 24% from the $(1s)^2(0d_{5/2})^2$ and 41% from the $(0d_{5/2})^4$ configuration. These $(1s)^2$ configurations also help to increase the neutron distribution radii. Consequently, ^{16}C and ^{18}C have much thicker neutron skin than ^{14}C. The question we will examine below is how this neutron skin affects the α clustering at nuclear surface.

3.2 α formation probability and neutron-skin thickness

Using the GCM wave functions explained above, we have evaluated the RWAs for the ground states of C isotopes, which are shown in Fig. 4.

As expected, the RWAs of the self-conjugate nucleus ^{12}C (Fig. 4, panel (a)) have the largest amplitude in all of the $\ell = 0$, 2 and 4 channels. The amplitudes of $\ell = 0$ and 2 are peaked at nuclear exterior ($r \geq 2.5$ fm), but oscillates and is suppressed in the interior due to the Pauli exclusion. The $\ell = 4$ amplitude peaks slightly inward because it has centrifugal barrier and no Pauli forbidden state. ^{14}C also has pronounced

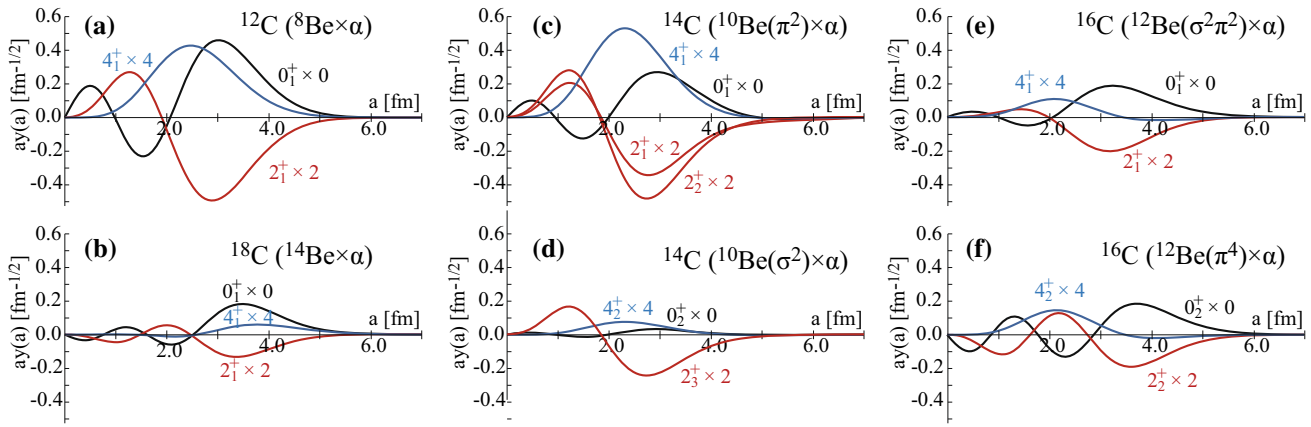

Fig. 4 The calculated α RWA of carbon isotopes in the $\ell_n^+ \times \ell$ channels, where ℓ_n^+ denotes the spin-parity of ^{A}Be while ℓ denotes orbital angular momentum between α and ^{A}Be. The **d** and **f** show the RWAs of ^{14}C and ^{16}C in the $\alpha + {}^A\text{Be}^*$ channels where Be isotopes are excited to the non-yrast states

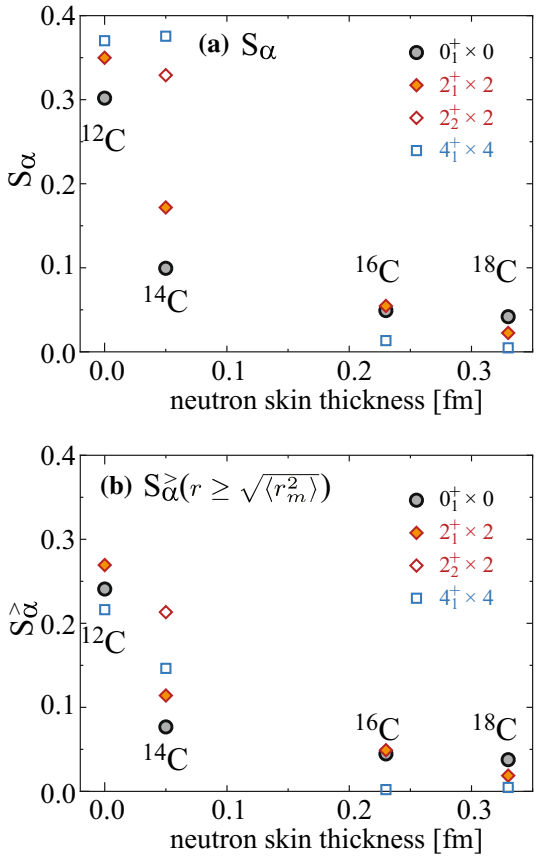

Fig. 5 **a** The calculated α spectroscopic factors as function of the neutron-skin thickness. **b** Same with the panel (**a**), but the RWAs are integrated in the nuclear exterior ($r \geq \sqrt{\langle r_m^2 \rangle}$)

RWAs (panel (c)) in the exterior region but they are slightly suppressed compared to ^{12}C. It is noted that ^{10}Be(2_2^+) state have almost the same intrinsic structure of ^{10}Be(0_1^+), and as a result, the RWA in the ^{10}Be(2_2^+) channel is also large. On the other hand, the RWAs in other non-yrast state channels, *i.e.* ^{10}Be($0_2^+, 2_3^+, 4_2^+$), are suppressed. This is due to the excited valence neutron configuration of ^{10}Be.

The RWAs of ^{16}C and ^{18}C show quite different behavior. They are strongly suppressed in both of the yrast (panels (b) and (e)) and the non-yrast (panel (f)) channels. Especially, the amplitudes are suppressed in the surface region where neutron skin exists. To quantitatively evaluate this suppression, Fig. 5 shows the α spectroscopic factors integrated over whole space (panel (a)) and those integrated in nuclear exterior (panel (b)) as function of neutron-skin thickness. It looks that the reduction of the α clustering correlates with the neutron-skin thickness, and this trend is consistent with the reduction of the $(p, p\alpha)$ knockout reaction cross section observed in Sn isotopes [8].

Here, we also make a couple of comments on the characteristics of the RWAs. First, most of the $\ell = 0$ and 2 RWAs are peaked at $a = 3.0$ to 3.5 fm at which nuclear density falls off less than 0.03 fm^{-3}. Interestingly, this density coincide with the value in Ref. [42], at which α cluster dissolves in the nuclear matter. At the moment, we cannot prove the reason behind this interesting coincidence, but we believe that more systematic analysis in heavier-mass system will give us deeper insight. Second, the $\ell = 4$ RWAs other than that of ^{18}C are peaked inside of nucleus. This is due to the lack of Pauli exclusion in $\ell = 4$ channel. By counting the principal quantum number of harmonic oscillator, we can find that the relationship $2n + \ell \geq 4$ must be satisfied in $^{12-16}$C, where n and ℓ denote the nodal quantum number and orbital angular momentum of RWA, respectively. Therefore, any non-negative value of the nodal quantum number is allowed for $\ell = 4$, i.e. there are no Pauli exclusion. On the other hand, the relationship is different in ^{18}C. It is $2n + \ell \geq 6$, hence $n = 0$ is forbidden for $\ell = 4$. Consequently, the RWA of ^{18}C is pushed outwards. Finally, in the panel (d), the RWA in the $2_3^+ \times 2$ channel is notably larger than those in the $\ell = 0$ and 4

channels. This may be due to the configuration mixing in the ^{10}Be(2_2^+) and ^{10}Be(2_3^+). Because the energies of these states are closer than the 0_1^+-0_2^+ and 4_1^+-4_2^+ pairs, stronger configuration mixing is induced. Therefore, ^{10}Be(2_3^+) has non-negligible ^{10}Be(π^2) configuration in addition to the dominant ^{10}Be(σ^2) configuration. Consequently, the RWA in the $2_3^+ \times 2$ channel becomes large comparable with that in the $2_2^+ \times 2$ channel.

Thus, the α clustering suppression by the growth of the neutron-skin likely also exists in light mass isotope chain. However, we also mention an alternative interpretation of Figs. 4 and 5. As we have already discussed, the neutron-skin thickness and the structure of the core nucleus (Be isotopes) are strongly dependent on the neutron single-particle configuration. Therefore, the neutron shell effect can be the real cause of the α clustering suppression observed in these figures. We should also consider the relationship between the α clustering and α threshold energy [43]. To identify the real cause of the α clustering suppression, the systematic study of other isotopes chains such as O, Ne and Mg isotopes is important, and the research is now undergoing.

4 Summary

In this study, we have investigated the relationship between the neutron-skin thickness and α clustering of C isotopes to elucidate the possible clustering suppression by neutron skin. The AMD framework has successfully described the low-lying spectra of both isotope chains simultaneously. Using the obtained wave functions, we have evaluated the neutron-skin thickness and α clustering. It has been shown that ^{16}C and ^{18}C have thick neutron skin, while ^{12}C and ^{14}C do not. The calculated α spectroscopic factors show the negative correlation with the neutron-skin thickness. Namely, α clustering is considerably suppressed in ^{16}C and ^{18}C. Thus, the growth of the neutron skin seems to suppress the α clustering of C isotopes similarly to those observed in Sn isotopes. However, we also point out that neutron shell effect may also play the crucial role and can be the real cause of the α clustering suppression. This will be clarified by investigating the trends in the neighboring isotopes chains.

Acknowledgements The ECT* Trento has supported this work and this infrastructure is part of a project that has received funding from the European Union's Horizon 2020 research and innovation programme under Grant Agreement No 824093. We also acknowledge that this work was also supported by the JSPS KAKENHI Grant No. 19K03859 and by the COREnet program at RCNP Osaka University. Part of the numerical calculations were performed using Oakforest-PACS at the Center for Computational Sciences in the University of Tsukuba.

Table 2 The dimensionless parameters for an approximate expression of the Coulomb interaction

n	c_n	γ_n
1	0.437686	8.888000
2	−0.421877	6.244998
3	0.363035	4.358899
4	0.082946	3.000000
5	0.179389	2.000000
6	0.717984	1.224745
7	2.108150	0.500000

Data Availability Statement This manuscript has no associated data or the data will not be deposited. [Authors' comment: Readers who need the data for Figs. 1–5 should contact the corresponding author, via e-mail.]

Appendix A: Coulomb interaction

To reduce the computational cost, the Coulomb interaction is approximated by a sum of seven Gaussians as

$$\frac{1}{r} \simeq \sum_{n=1}^{7} c_n \sqrt{\bar{\nu}} \exp\left(-\frac{\bar{\nu} r^2}{\gamma_n^2}\right), \quad \bar{\nu} = (\nu_x \nu_y \nu_z)^{1/3}, \tag{A.1}$$

where the dimensionless parameters c_n and γ_n are listed in Table 2. The parameters are determined to yield approximate values of the Coulomb interaction when the matrix elements of Eq. (A.1) are calculated from the nucleon Gaussian wave packets.

References

1. S. Typel, G. Röpke, T. Klähn, D. Blaschke, H.H. Wolter, Phys. Rev. C **81**, 015803015803 (2010)
2. K. Hagel, R. Wada, L. Qin, J.B. Natowitz, S. Shlomo, A. Bonasera, G. Röpke, S. Typel, Z. Chen, M. Huang, J. Wang, H. Zheng, S. Kowalski, C. Bottosso, M. Barbui, M.R.D. Rodrigues, K. Schmidt, D. Fabris, M. Lunardon, S. Moretto, G. Nebbia, S. Pesente, V. Rizzi, G. Viesti, M. Cinausero, G. Prete, T. Keutgen, Y. El Masri, Z. Majka, Phys. Rev. Lett. **108**, 062702 (2012)
3. S. Typel, Phys. Rev. C **89**, 064321 (2014)
4. K. Yoshida, K. Minomo, K. Ogata, Phys. Rev. C **94**, 044604 (2016)
5. T. Wakasa, K. Ogata, T. Noro, Prog. Part. Nucl. Phys. **96**, 32 (2017)
6. K. Yoshida, K. Ogata, Y. Kanada-En'Yo, Phys. Rev. C **98**, 024614 (2018)
7. K. Yoshida, Y. Chiba, M. Kimura, Y. Taniguchi, Y. Kanada-En'Yo, K. Ogata, Phys. Rev. C **100**, 044601 (2019)
8. J. Tanaka, Z. Yang, S. Typel, S. Adachi, S. Bai, P. van Beek, D. Beaumel, Y. Fujikawa, J. Han, S. Heil, S. Huang, A. Inoue, Y. Jiang, M. Knösel, N. Kobayashi, Y. Kubota, W. Liu, J. Lou, Y. Maeda, Y. Matsuda, K. Miki, S. Nakamura, K. Ogata, V. Panin, H. Scheit, F. Schindler, P. Schrock, D. Symochko, A. Tamii, T. Uesaka, V. Wagner, K. Yoshida, J. Zenihiro, T. Aumann, Science **371**, 260 (2021)
9. R.G. Lovas, R.J. Liotta, A. Insolia, K. Varga, D.S. Delion, Phys. Rep. **294**, 265 (1998)

10. C. Qi, R. Liotta, R. Wyss, Prog. Part. Nucl. Phys. **105**, 214 (2019)
11. W. von Oertzen, M. Freer, Y. Kanada-En'yo, Phys. Rep. **432**, 43 (2006)
12. Y. Kanada-En'yo, M. Kimura, A. Ono, Progress Theor. Exp. Phys. **2012**, 1A202 (2012)
13. M. Kimura, T. Suhara, Y. Kanada-En'yo, Eur. Phys. J. A **52**, 373 (2016)
14. A. Tohsaki, H. Horiuchi, P. Schuck, G. Röpke, Phys. Rev. Lett. **87**, 192501 (2001)
15. Y. Funaki, A. Tohsaki, H. Horiuchi, P. Schuck, G. Röpke, Phys. Rev. C **67**, 051306 (2003)
16. P. Schuck, Y. Funaki, H. Horiuchi, G. Röpke, A. Tohsaki, T. Yamada, Phys. Scr. **91**, 23001 (2016)
17. B. Zhou, A. Tohsaki, H. Horiuchi, Z. Ren, Phys. Rev. C **94**, 044319 (2016)
18. Y. Kanada-En'yo, M. Kimura, H. Horiuchi, C.R. Phys. **4**, 497 (2003)
19. J. Berger, M. Girod, D. Gogny, Comput. Phys. Commun. **63**, 365 (1991)
20. M. Kimura, Phys. Rev. C **69**, 044319 (2004)
21. M. Kimura, R. Yoshida, M. Isaka, Progress Theor. Phys. **127**, 287 (2012)
22. D.L. Hill, J.A. Wheeler, Phys. Rev. **89**, 1102 (1953)
23. Y. Chiba, M. Kimura, Progress Theor. Exp. Phys. **2017**, 053D01 (2017)
24. N. Imai, H.J. Ong, N. Aoi, H. Sakurai, K. Demichi, H. Kawasaki, H. Baba, Z. Dombrádi, Z. Elekes, N. Fukuda, Z. Fülöp, A. Gelberg, T. Gomi, H. Hasegawa, K. Ishikawa, H. Iwasaki, E. Kaneko, S. Kanno, T. Kishida, Y. Kondo, T. Kubo, K. Kurita, S. Michimasa, T. Minemura, M. Miura, T. Motobayashi, T. Nakamura, M. Notani, T.K. Onishi, A. Saito, S. Shimoura, T. Sugimoto, M.K. Suzuki, E. Takeshita, S. Takeuchi, M. Tamaki, K. Yamada, K. Yoneda, H. Watanabe, M. Ishihara, Phys. Rev. Lett. **92**, 062501 (2004)
25. H.J. Ong, N. Imai, D. Suzuki, H. Iwasaki, H. Sakurai, T.K. Onishi, M.K. Suzuki, S. Ota, S. Takeuchi, T. Nakao, Y. Togano, Y. Kondo, N. Aoi, H. Baba, S. Bishop, Y. Ichikawa, M. Ishihara, T. Kubo, K. Kurita, T. Motobayashi, T. Nakamura, T. Okumura, Y. Yanagisawa, Phys. Rev. C **78**, 014308 (2008)
26. M. Petri, S. Paschalis, R.M. Clark, P. Fallon, A.O. MacChiavelli, K. Starosta, T. Baugher, D. Bazin, L. Cartegni, H.L. Crawford, M. Cromaz, U. Datta Pramanik, G. De Angelis, A. Dewald, A. Gade, G.F. Grinyer, S. Gros, M. Hackstein, H.B. Jeppesen, I.Y. Lee, S. McDaniel, D. Miller, M.M. Rajabali, A. Ratkiewicz, W. Rother, P. Voss, K.A. Walsh, D. Weisshaar, M. Wiedeking, B.A. Brown, C. Forssén, P. Navrátil, R. Roth, Physical Review C **86**, 044329 (2012)
27. P. Voss, T. Baugher, D. Bazin, R.M. Clark, H.L. Crawford, A. Dewald, P. Fallon, A. Gade, G.F. Grinyer, H. Iwasaki, A.O. MacChiavelli, S. McDaniel, D. Miller, M. Petri, A. Ratkiewicz, W. Rother, K. Starosta, K.A. Walsh, D. Weisshaar, C. Forssén, R. Roth, P. Navrátil, Phys. Rev. C **86**, 011303 (2012)
28. F. Ajzenberg-Selove, Nucl. Phys. Sect. A **523**, 1 (1991)
29. D.R. Tilley, J.H. Kelley, J.L. Godwin, D.J. Millener, J.E. Purcell, C.G. Sheu, H.R. Weller, Nucl. Phys. A **745**, 155 (2004)
30. J.H. Kelley, J.E. Purcell, C.G. Sheu, Nucl. Phys. A **968**, 71 (2017)
31. F. Ajzenberg-Selove, Nucl. Phys. Sect. A **460**, 1 (1986)
32. D.R. Tilley, H.R. Weller, C.M. Cheves, R.M. Chasteler, Nucl. Phys. Sect. A **595**, 1 (1995)
33. W. von Oertzen, Zeitschrift für Physik A Hadrons and Nuclei **354**, 37 (1996)
34. W. von Oertzen, Il Nuovo Cimento A **110**, 895 (1997)
35. I. Talmi, I. Unna, Phys. Rev. Lett. **4**, 469 (1960)
36. N. Itagaki, S. Hirose, T. Otsuka, S. Okabe, K. Ikeda, Phys. Rev. C **65**, 6 (2002)
37. Y. Kanada-En'yo, Phys. Rev. C **71**, 014310 (2005)
38. Y. Jiang, J.L. Lou, Y.L. Ye, Y. Liu, Z.W. Tan, W. Liu, B. Yang, L.C. Tao, K. Ma, Z.H. Li, Q.T. Li, X.F. Yang, J.Y. Xu, H.Z. Yu, J.X. Han, S.W. Bai, S.W. Huang, G. Li, H.Y. Wu, H.L. Zang, J. Feng, Z.Q. Chen, Y.D. Chen, Q. Yuan, J.G. Li, B.S. Hu, F.R. Xu, J.S. Wang, Y.Y. Yang, P. Ma, Q. Hu, Z. Bai, Z.H. Gao, F.F. Duan, L.Y. Hu, J.H. Tan, S.Q. Sun, Y.S. Song, H.J. Ong, D.T. Tran, D.Y. Pang, C.X. Yuan, Phys. Rev. C **101**, 024601 (2020)
39. Z. Elekes, Z. Dombrádi, A. Krasznahorkay, H. Baba, M. Csatlós, L. Csige, N. Fukuda, Z. Fülöp, Z. Gácsi, J. Gulyás, N. Iwasa, H. Kinugawa, S. Kubono, M. Kurokawa, X. Liu, S. Michimasa, T. Minemura, T. Motobayashi, A. Ozawa, A. Saito, S. Shimoura, S. Takeuchi, I. Tanihata, P. Thirolf, Y. Yanagisawa, K. Yoshida, Phys. Lett. Sect. B **586**, 34 (2004)
40. V. Choudhary, W. Horiuchi, M. Kimura, R. Chatterjee, Phys. Rev. C **102**, 034619 (2020)
41. S. Karataglidis, K. Murulane, Phys. Rev. C **101**, 064316 (2020)
42. G. Röpke, P. Schuck, Y. Funaki, H. Horiuchi, Z. Ren, A. Tohsaki, C. Xu, T. Yamada, B. Zhou, Phys. Rev. C **90**, 034304 (2014)
43. K. Ikeda, N. Takigawa, H. Horiuchi, Progress Theor. Phys. Supplement **E68**, 464 (1968)